J. Fluid Mech. (1975), *vol.* 69, *part* 2, *pp.* 377–403
Printed in Great Britain

Stokes flow past a particle of arbitrary shape: a numerical method of solution

By G. K. YOUNGREN AND A. ACRIVOS

Department of Chemical Engineering, Stanford University, Stanford, California 94305

(Received 25 February 1974 and in revised form 13 November 1974)

The problem of determining the slow viscous flow of an unbounded fluid past a single solid particle is formulated exactly as a system of linear integral equations of the first kind for a distribution of Stokeslets over the particle surface. The unknown density of Stokeslets is identical with the surface-stress force and can be obtained numerically by reducing the integral equations to a system of linear algebraic equations. This appears to be an efficient way of determining solutions for several external flows past a particle, since it requires that the matrix of the algebraic system be inverted only once for a given particle.

The technique was tested successfully against the analytic solutions for spheroids in uniform and simple shear flows, and was then applied to two problems involving the motion of finite circular cylinders: (i) a cylinder translating parallel to its axis, for which the local stress force distribution and the drag were determined; and (ii) the equivalent axis ratio of a freely suspended cylinder, which was calculated by determining the couple on a stationary cylinder placed symmetrically in two different simple shear flows. The numerical results were found to be consistent with the asymptotic analysis of Cox (1970, 1971) and in excellent agreement with the experiments of Anczurowski & Mason (1968), but not with those of Harris & Pittman (1975).

1. Introduction

Although the classical Stokes-flow problem of the motion of an inertialess unbounded fluid past a single body has been studied for more than 100 years, analytical solutions have been obtained only for special geometries. For example, Stokes (1851) solved the problem of a translating sphere, Oberbeck (1876) extended this result to an ellipsoid translating parallel to its axis, while Jeffery (1922) obtained the solution for an ellipsoid immersed in a general linear flow field. More recently, solutions have been derived for bodies which correspond to a co-ordinate surface of one of the special orthogonal co-ordinate systems in which the Stokes equations are simply separable (see Payne & Pell 1960; Nir & Acrivos 1973). Additionally, Stokes-flow theory has been extensively developed for flow past long slender bodies (Batchelor 1970; Cox 1970, 1971) and for flow past slightly deformed spheres (Taylor & Acrivos 1964; Brenner 1964*a*).

No analytic solutions are at present available, however, for general body shapes and, indeed, none has been found for the apparently simple geometry of

a cylinder translating parallel to its axis. Thus, to describe Stokes flow past general bodies, it is usually necessary to resort to a numerical approach.

Of course, it should in principle be possible to use a conventional finite-difference scheme, but unfortunately the integration domain would have to be made very large relative to the particle size since the absence of any inertial effects results in slow algebraic decay in all directions of any disturbance produced by the body. Gluckman, Weinbaum & Pfeffer (1972) presented two striking illustrations of this effect and concluded that it would normally be impractical to employ finite-difference methods for infinite-domain Stokes problems.

Fortunately, the linearity of the Stokes equations suggests an approach based on superposition to take advantage of this linearity, and indeed, considerable work has been done using different schemes based on the method of weighted residuals. Thus, for axisymmetric flow past nearly spherical particles, O'Brien (1968) expanded the stream function as a truncated power series in Sampson's (1891) separable solutions written in spherical co-ordinates and, using a boundary collocation method (Finlayson 1972, p. 11), satisfied the no-slip boundary condition at selected collocation points. Similarly, for flow past a three-dimensional, nearly spherical particle, Rosen (1972) expressed the velocity field in terms of Lamb's (1932, p. 595) general solution, truncated the series and minimized the mean-square error in satisfying the no-slip condition. However, the range of validity of weighted residual methods is limited, as was illustrated by Gluckman *et al.* (1972), who attempted to extend O'Brien's approach to more elongated spheroids and found that, for a prolate spheroid with an axis ratio of 2·0, the numerically calculated drag oscillated unstably as the number of collocation points was increased. This difficulty was resolved by Bowen & Masliyah (1973), who expressed the stream function in terms of Sampson's separable solutions written in spheroidal co-ordinates and performed a least-squares fit to satisfy approximately the no-slip condition. With this technique, numerically calculated values of the drag for extended spheroids compared very well with the exact analytical results. Nevertheless, it is not clear how well this method would succeed with particles which are not approximately spheroidal.

Using a slightly different approach, Gluckman *et al.* (1972) observed that any convex body of revolution may be approximated by a finite number of touching oblate spheroids with very large aspect ratios. Since the solution for axisymmetric flow past an individual oblate spheroid is given by an infinite series of Legendre polynomials (Sampson 1891), by superposition, the flow past the assembly of spheroids can be expressed as a double sum. By truncating the infinite series and employing a boundary collocation scheme, Gluckman *et al.* obtained an approximate solution for which the computed drag agreed very well with the analytical results for spheroids. Drag results for cylinders and cones were also presented.

Thus, a number of numerical schemes have been proposed for axisymmetric flows past axisymmetric bodies which are either convex or approximately spheroidal, or for three-dimensional flows past nearly spherical bodies, but none of these methods is general in the sense that it can handle each of these three

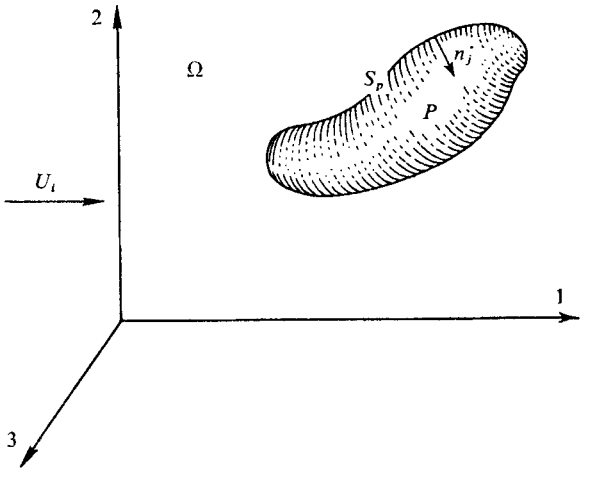

FIGURE 1. Stokes flow past an arbitrary particle.

problems or, which is of even more significance, the general three-dimensional case.

The work of Hunt (1968) and Smith & Hess (1966) on potential flow, Cruse (1969) in elastostatics and Chang, Kang & Chen (1973) on heat conduction suggests, however, that an integral-equation approach to the Stokes problem might be appropriate. In this method, the fundamental singular solutions of the governing differential equations are continuously distributed over the boundaries of the problem, and the boundary conditions then lead to integral equations for the densities of the fundamental solutions. Thus, the solution of a differential equation in n dimensions is reduced to the solution of an integral equation in $n-1$ dimensions. In addition to reducing the dimensions of the problem, this method is attractive for Stokes problems since it is a very general approach independent of the body geometry and the form of the external flow field. To be sure, analytical solution of the integral equations is, in general, not possible, but these can be solved numerically. The philosophy and advantages of recasting the solution in integral form were discussed in detail by Gluckman *et al.* (1972), who described such an approach (though they did not use the fundamental singular solution) for axisymmetric flow past convex bodies although, in the end, they only made use of the aforementioned collocation procedure for their numerical experiments.

2. Formulation of problem

The problem of creeping flow in a domain Ω past an arbitrary particle P with surface S_p (figure 1) is described by

$$\frac{\partial^2 v_i(\mathbf{x})}{\partial x_j \partial x_j} = \frac{\partial p(\mathbf{x})}{\partial x_i}, \quad \frac{\partial v_i(\mathbf{x})}{\partial x_i} = 0, \quad \mathbf{x} \in \Omega, \tag{2.1}$$

$$v_i(\mathbf{x}) = -U_i(\mathbf{x}), \quad \mathbf{x} \in S_p,$$

$$v_i(\mathbf{x}), p(\mathbf{x}) \to 0 \quad \text{as} \quad |\mathbf{x}| \to \infty, \tag{2.2}$$

where all the variables are dimensionless and the usual Cartesian tensor summation convention is adopted. The reduction of the solution of (2.1) and (2.2) to the solution of a system of integral equations is well known and, as described by Ladyzhenskaya (1963, p. 49), forms the basis of Odqvist's (1930) proof of the existence and uniqueness of a solution to (2.1) and (2.2).

The fundamental singular solution of (2.1) is

$$\left.\begin{aligned} u_{ij}(\mathbf{x},\mathbf{y}) &= \frac{-1}{8\pi}\left[\frac{\delta_{ij}}{r_{xy}}+\frac{(x_i-y_i)(x_j-y_i)}{r_{xy}^3}\right], \\ p_j(\mathbf{x},\mathbf{y}) &= (y_j-x_j)/4\pi r_{xy}^3, \end{aligned}\right\} \tag{2.3}$$

where $r_{xy} = |\mathbf{x}-\mathbf{y}|$. It is clear that, as a function of $\mathbf{x}$, (2.3) solves (2.1) for $\mathbf{x} \neq \mathbf{y}$ and has the appropriate singular behaviour at $\mathbf{x} = \mathbf{y}$. Physically, $u_{ij}(\mathbf{x},\mathbf{y})$ represents the ith velocity component at $\mathbf{x}$ due to a unit force (commonly referred to as a Stokeslet) in the j direction applied at $\mathbf{y}$, while p_j represents the associated pressure at $\mathbf{x}$.

Next, by defining the shear-stress tensor $\{T_{ij}\}$,

$$T_{ij}(\mathbf{v}) = -\delta_{ij}p+\partial v_i/\partial x_j+\partial v_j/\partial x_i, \tag{2.4}$$

and using the divergence theorem, one can easily obtain what might be called Green's formula for the Stokes problem for smooth solenoidal vectors $\mathbf{u}$ and $\mathbf{v}$ and smooth scalars p and q in the bounded domain E with boundary ∂E:

$$\begin{aligned} \iiint_E \left\{v_i(\mathbf{x})\left[\frac{\partial^2 u_i(\mathbf{x})}{\partial x_j\,\partial x_j}-\frac{\partial q}{\partial x_i}\right]-u_i(\mathbf{x})\left[\frac{\partial^2 v_i(\mathbf{x})}{\partial x_j\,\partial x_j}-\frac{\partial p}{\partial x_i}\right]\right\} d\mathbf{x} \\ = \iint_{\partial E}\{v_i(\mathbf{x})\,T_{ij}[\mathbf{u}(\mathbf{x})]\,n_j(\mathbf{x})-u_i(\mathbf{x})\,T_{ij}[\mathbf{v}(\mathbf{x})]\,n_j(\mathbf{x})\}\,dS_x, \end{aligned} \tag{2.5}$$

where $T_{ij}[\mathbf{u}(\mathbf{x})] = -\delta_{ij}q+\partial u_i/\partial x_j+\partial u_j/\partial x_i$ and where dS_x indicates that the integration over ∂E is with respect to the point $\mathbf{x}$. Then, by replacing (u_i, q) with the fundamental solutions (u_{ij}, p_j), identifying v_i and p with the solution to (2.1) and using the facts that $v_i(\mathbf{x}) = O(|\mathbf{x}|^{-1})$ and $p(\mathbf{x}) = O(|\mathbf{x}|^{-2})$ as $|\mathbf{x}| \to \infty$, Green's representation formula (or Green's third identity) for the Stokes problem follows readily:

$$\left.\begin{aligned} v_i(\mathbf{x}) &= V_i^{(1)}(\mathbf{x})+V_i^{(2)}(\mathbf{x}), \\ p(\mathbf{x}) &= P^{(1)}(\mathbf{x})+P^{(2)}(\mathbf{x}), \end{aligned}\right\} \quad \mathbf{x}\in\Omega, \tag{2.6}$$

where

$$\begin{aligned} V_i^{(1)}(\mathbf{x}) &= -\iint_{S_p} u_{ik}(\mathbf{x},\mathbf{y})\,T_{kj}[\mathbf{v}(\mathbf{y})]\,n_j(\mathbf{y})\,dS_y \\ &\equiv -\iint_{S_p} u_{ik}(\mathbf{x},\mathbf{y})f_k(\mathbf{y})\,dS_y, \quad \mathbf{x}\in\Omega, \end{aligned} \tag{2.7a}$$

$$V_i^{(2)}(\mathbf{x}) = \frac{-3}{4\pi}\iint_{S_p}\frac{(x_i-y_i)(x_j-y_j)(x_k-y_k)\,v_k(\mathbf{y})\,n_j(\mathbf{y})}{r_{xy}^5}\,dS_y, \quad \mathbf{x}\in\Omega, \tag{2.7b}$$

$$\begin{aligned} P^{(1)}(\mathbf{x}) &= -\iint_{S_p} p_k(\mathbf{x},\mathbf{y})\,T_{kj}[\mathbf{v}(\mathbf{y})]\,n_j(\mathbf{y})\,dS_y \\ &\equiv -\iint_{S_p} p_k(\mathbf{x},\mathbf{y})f_k(\mathbf{y})\,dS_y, \quad \mathbf{x}\in\Omega, \end{aligned} \tag{2.7c}$$

$$P^{(2)}(\mathbf{x}) = \frac{1}{2\pi}\iint_{S_p}\left[\frac{\delta_{kj}}{r_{xy}^3} - \frac{3(x_k-y_k)(x_j-y_j)}{r_{xy}^5}\right] v_k(\mathbf{y})\, n_j(\mathbf{y})\, dS_y, \quad \mathbf{x}\in\Omega, \quad (2.7d)$$

$$f_k(\mathbf{y}) \equiv T_{kj}[\mathbf{v}(\mathbf{y})]\, n_j(\mathbf{y}). \quad (2.7e)$$

$(V_i^{(1)}, P^{(1)})$ and $(V_i^{(2)}, P^{(2)})$ are termed single and double-layer potentials, with densities f_k and v_k respectively by analogy with the corresponding potentials from potential theory. f_k is the local surface-stress force and n_j is the *inward* normal to the particle.

The combinations $(V_i^{(1)}(\mathbf{x}), P^{(1)}(\mathbf{x}))$ and $(V_i^{(2)}(\mathbf{x}), P^{(2)}(\mathbf{x}))$ individually satisfy (2.1) for $\mathbf{x}\in\Omega$ and thus (2.6) is a solution of (2.1). Furthermore, since $V_i^{(1)}(\mathbf{x})$, $V_i^{(2)}(\mathbf{x})$, $P^{(1)}(\mathbf{x})$ and $P^{(2)}(\mathbf{x})$ all tend to zero at infinity, it only remains to satisfy the no-slip condition. Odqvist showed that if one attempts to express $v_i(\mathbf{x})$ solely in terms of double-layer potentials (with densities not, in general, equal to v_k), the integral equation of the second kind that results on applying the no-slip condition has six eigensolutions. Thus, in general, $v_i(\mathbf{x})$ cannot be represented in terms of double-layer potentials alone, but rather must be written in terms of the six single-layer potentials, with the eigensolutions of the adjoint integral equation as densities, plus the double-layer potentials. However, since the eigensolutions of the adjoint equation are in general unknown, this approach is not convenient for computational purposes. Although such a difficulty does not result if $v_i(\mathbf{x})$ is written using only single-layer potentials with density ψ_k (or, stated in more familiar terms, as a distribution of Stokeslets over the particle surface), the essentially equivalent approach of deriving the appropriate integral equations starting with (2.6), thus retaining the double-layer potential terms, will be employed here since this identifies the unknown densities in the resulting integral equations with the local stress force f_k.

The single-layer potentials $V_i^{(1)}(\mathbf{x})$ are continuous in the entire space if the densities f_k are continuous, which will be true if S_p is, as will be assumed, a Lyapunov surface (Günter 1967, p. 7; for surfaces of practical interest this requires the surface to have a well-defined tangent plane at all points). However, the double-layer potentials $V_i^{(2)}(\mathbf{x})$ are not continuous at S_p but suffer a jump given by (Odqvist 1930)

$$\lim_{\mathbf{x}\to\mathbf{x}_0} V_i^{(2)}(\mathbf{x}) = V_i^{(2)}(\mathbf{x}_0) + \tfrac{1}{2}v_i(\mathbf{x}_0), \quad \mathbf{x}\in\Omega, \quad \mathbf{x}_0\in S_p. \quad (2.8)$$

Using these facts, the no-slip condition leads then to the following linear integral equations of the first kind for the densities f_k:

$$-U_i(\mathbf{x}) = \frac{3}{2\pi}\iint_{S_p}\frac{(x_i-y_i)(x_j-y_j)(x_k-y_k)\, n_j(\mathbf{y})\, U_k(\mathbf{y})}{r_{xy}^5} dS_y + \frac{1}{4\pi}\iint_{S_p}\left[\frac{\delta_{ik}}{r_{xy}} + \frac{(x_i-y_i)(x_k-y_k)}{r_{xy}^3}\right] f_k(\mathbf{y})\, dS_y, \quad \mathbf{x}\in S_p. \quad (2.9)$$

It is not difficult to see that the integrals in these equations, though improper for $\mathbf{x} = \mathbf{y}$, do exist if S_p is a Lyapunov surface. Since, as shown in appendix A, equations (2.9) have a unique solution for all $U_i(\mathbf{x})$, it follows that the solution of (2.1) and (2.2) has been reduced to the solution of (2.9).

Thus when the Stokes problem is formulated in this manner, the stress force

distribution, which is normally the quantity of interest in such calculations, is determined directly. This is in contrast to other methods, which yield directly the coefficients in a (truncated) infinite series for the velocity or stream function, coefficients which normally are of only limited quantitative importance. Furthermore, as shown in §4, the present method yields accurate *local* stress forces f_i, whereas the success of other schemes has only been demonstrated to date in terms of computed integral properties such as the drag.

Equations (2.9) simplify for the cases of uniform flow at infinity and axisymmetric flow. Specifically, if $U_i(\mathbf{x})$ is a constant W_i, then it can be shown using (2.5) that

$$\frac{3}{2\pi}\iint_{S_p}\frac{(x_i-y_i)(x_j-y_j)(x_k-y_k)n_j(\mathbf{y})W_k}{r_{xy}^5}dS_y = W_i, \quad \mathbf{x}\in S_p, \tag{2.10}$$

and hence (2.9) reduces to

$$W_i = \frac{-1}{8\pi}\iint_{S_p}\left[\frac{\delta_{ik}}{r_{xy}}+\frac{(x_i-y_i)(x_k-y_k)}{r_{xy}^3}\right]f_k(\mathbf{y})\,dS_y, \quad \mathbf{x}\in S_p. \tag{2.11}$$

It is of interest to point out that, had the velocity field been expressed solely in terms of single-layer potentials, (2.11) would have followed immediately since, as noted above, the single-layer potentials are continuous across S_p. However, the above arguments serve to show that the densities of the potential layers in (2.11) are equal to the surface-stress force.

For uniform flow at infinity in direction 1 parallel to the axis of an axisymmetric body, (2.11) reduces to a one-dimensional integral equation. Specifically if the uniform flow has speed W_1, if f_r is the radial component of $\mathbf{f}$ in a cylindrical co-ordinate system with axis in the 1 direction and if the particle surface in terms of cylindrical co-ordinates is given by

$$y_2 = R(y_1)\cos\theta, \quad y_3 = R(y_1)\sin\theta, \tag{2.12}$$

where $-1 \leqslant y_1 \leqslant 1, R(\pm 1) = 0$ and $R(y_1)$ is single valued, then the integration in the azimuthal direction can be performed analytically. Thus, setting

$$k = \left[\frac{4R(x_1)R(y_1)}{(x_1-y_1)^2+\{R(x_1)+R(y_1)\}^2}\right]^{\frac{1}{2}} \tag{2.13}$$

we obtain from (2.11)

$$\begin{aligned} W_1 = {} & \frac{-1}{4\pi}\int_{-1}^{1} kR^{-\frac{1}{2}}(x_1)R^{\frac{1}{2}}(y_1)f_1(y_1)\{1+R'^2\}\{F+(x_1-y_1)^2E/r_{xy}^2\}dy_1 \\ & +\frac{1}{8\pi}\int_{-1}^{1} kR^{-\frac{1}{2}}(x_1)R^{-\frac{1}{2}}(y_1)f_r(y_1)(x_1-y_1)\{1+R'^2\} \\ & \times\{F+[R^2(x_1)-R^2(y_1)+(x_1-y_1)^2]E/r_{xy}^2\}dy_1, \quad -1\leqslant x_1\leqslant 1, \end{aligned} \tag{2.14a}$$

and

$$\begin{aligned} 0 = {} & \frac{1}{4\pi}\int_{-1}^{1} kR^{-\frac{3}{2}}(x_1)R^{\frac{1}{2}}(y_1)f_1(y_1)(x_1-y_1)\{1+R'^2\} \\ & \times\{F+[R^2(x_1)-R^2(y_1)-(x_1-y_1)^2]E/r_{xy}^2\}dy_1+\frac{1}{4\pi}\int kR^{-\frac{3}{2}}(x_1)R^{-\frac{1}{2}}(y_1) \\ & \times f_r(y_1)\{1+R'^2\}\{[R^2(x_1)+R^2(y_1)+2(x_1-y_1)^2]F-[2(x_1-y_1)^4 \\ & +3(x_1-y_1)^2(R^2(x_1)+R^2(y_1))+(R^2(x_1)-R^2(y_1))^2]E/r_{xy}^2\}dy_1, \\ & -1\leqslant x_1\leqslant 1, \end{aligned} \tag{2.14b}$$

where $R' = dR/dy_1$, and F and E are, respectively, the complete elliptic integrals of the first and second kind with modulus k.

3. Numerical solution

Equations (2.9) and (2.14) can be solved numerically using the Krylov–Bogoliubov method (Kantorovich & Krylov 1958, p. 130), which transforms the integral equations into a linear system of algebraic equations. This is accomplished by dividing S_p into N elements $\Delta_m (m = 1, 2, \ldots, N)$ all of which are small relative to S_p and over which the components of $\mathbf{f}$ may, for the purposes of the integral equations, be considered constant and equal to their value at the centre of the element. The integral equations are satisfied at the centres $\mathbf{x}^{(m)} (m = 1, 2, \ldots, N)$ of each element, thereby yielding the numerical approximations to (2.9):

$$-U_i(\mathbf{x}^{(m)}) - \frac{3}{2\pi}\iint_{S_p} \frac{(x_i^{(m)} - y_i)(x_j^{(m)} - y_j)(x_k^{(m)} - y_k) n_j(\mathbf{y}) U_k(\mathbf{y})}{r_{x^{(m)}y}^5} dS_y$$
$$= \frac{1}{4\pi} \sum_{j=1}^{N} f_k(\mathbf{x}^{(j)}) \iint_{\Delta_j} \left[\frac{\delta_{ik}}{r_{x^{(m)}y}} + \frac{(x_i^{(m)} - y_i)(x_k^{(m)} - y_k)}{r_{x^{(m)}y}^3}\right] dS_y,$$

or
$$g_i(\mathbf{x}^{(m)}) = \sum_{j=1}^{N} A_{ik}^{(j)} f_k(\mathbf{x}^{(j)}) \quad (m = 1, 2, \ldots, N), \tag{3.1}$$

where

$$g_i(\mathbf{x}^{(m)}) \equiv -U_i(\mathbf{x}^{(m)}) - \frac{3}{2\pi}\iint_{S_p} \frac{(x_i^{(m)} - y_i)(x_j^{(m)} - y_j)(x_k^{(m)} - y_k) n_j(\mathbf{y}) U_k(\mathbf{y})}{r_{x^{(m)}y}^5} dS_y$$

and
$$A_{ik}^{(j)} \equiv \frac{1}{4\pi}\iint_{\Delta_j} \left[\frac{\delta_{ik}}{r_{x^{(m)}y}} + \frac{(x_i^{(m)} - y_i)(x_k^{(m)} - y_k)}{r_{x^{(m)}y}^3}\right] dS_y.$$

The above form a linear system of $3N$ equations in the $3N$ unknowns $f_k(\mathbf{x}^{(m)})$. Similarly, the axisymmetric case is approximated by a $2N \times 2N$ system which is easily obtained from (2.14). In either case the algebraic system can be solved numerically using suitable integration and matrix inversion techniques.

Even though, in deriving (2.9), it was necessary to assume that S_p was a Lyapunov surface, no such restriction on S_p is required to obtain (3.1), the discrete approximation. Indeed, each equation in (3.1) could have been obtained individually by taking the limit of (2.6) as $\mathbf{x}$ (in Ω) approached each $\mathbf{x}^{(m)}$ under the milder restriction that S_p be smooth in the sense of Lyapunov at each $\mathbf{x}^{(m)}$. This local Lyapunov condition also ensures that all the integrals in (3.1) exist. Therefore (3.1) applies to any particle which satisfies the Lyapunov conditions at each $\mathbf{x}^{(m)}$.

Since the density f_i is the local surface-stress force, the total force F_i and the couple T_i acting on the particle are, respectively,

$$F_i = -\sum_{=1}^{N} f_i(\mathbf{x}^{(j)}) \iint_{\Delta_j} dS_y, \quad T_i = \sum_{j=1}^{N} f_k(\mathbf{x}^{(j)}) \iint_{\Delta_j} \epsilon_{ilk} y_l dS_y, \tag{3.2}$$

while the velocity and pressure fields are given by, respectively,

$$\left.\begin{aligned} v_i(\mathbf{x}) = &-\sum_{j=1}^{N} f_k(\mathbf{x}^{(j)}) \iint_{\Delta_j} u_{ik}(\mathbf{x},\mathbf{y})\, dS_y \\ &+\frac{3}{4\pi}\iint_{S_p} \frac{(x_i-y_i)(x_j-y_j)(x_k-y_k)\, U_k(\mathbf{y})\, n_j(\mathbf{y})}{r_{xy}^5}\, dS_y, \\ p(\mathbf{x}) = &-\sum_{j=1}^{N} f_k(\mathbf{x}^{(j)}) \iint_{\Delta_j} p_k(\mathbf{x},\mathbf{y})\, dS_y \\ &-\frac{1}{2\pi}\iint_{S_p}\left[\frac{\delta_{kj}}{r_{xy}^3} - \frac{3(x_k-y_k)(x_j-y_j)}{r_{xy}^5}\right] U_k(\mathbf{y})\, n_j(\mathbf{y})\, dS_y, \end{aligned}\right\} \quad \mathbf{x}\in\Omega. \qquad (3.3)$$

The most critical feature of the numerical solution is the accurate calculation of the various surface integrals over the elements Δ_m, since it is these integrals which are the coefficients of the $f_k(\mathbf{x}^{(m)})$ in the algebraic system. These integrals are sensitive functions of position for small $r_{x^{(m)}y}$ and are improper at $\mathbf{y} = \mathbf{x}^{(m)}$.

For a general three-dimensional particle, the co-ordinate system is first transformed to allow a simplification in the expression for the surface integrals. A cylindrical co-ordinate system with azimuthal angle θ will be assumed for the purposes of this discussion. The direction of the axis is completely arbitrary and will be referred to as the 1 direction. The surface is next divided into N elements Δ_m whose boundaries are lines of constant x_1 and constant θ. In this way the surface elements become rectangular in x_1, θ co-ordinates, which is advantageous for two reasons. First, it simplifies the numerical calculation of the surface integrals since simple product integration schemes, based on any one-dimensional rule, are easily constructed for rectangular elements, and second, it is not necessary to give a precise definition of $\mathbf{x}^{(m)}$, the centre of Δ_m, since all reasonable definitions yield the geometric centre of the rectangle, a feature which does not necessarily hold for elements of arbitrary geometry. The numerical calculation of the surface integrals then presents no problems except when $j = m$, in which case the integrals are improper since the integration is carried out over the element which contains $\mathbf{x}^{(m)}$. In this case, the integration is divided into two regions: integration over a small neighbourhood of $\mathbf{x}^{(m)}$, whose exact dimensions are described below, and integration over the remainder of Δ_m. To perform the crucial integration over the neighbourhood of $\mathbf{x}^{(m)}$, the surface is assumed to be locally flat, i.e. it is approximated by the tangent plane at $\mathbf{x}^{(m)}$. Then, by transforming to a local polar co-ordinate system lying in this tangent plane with origin at $\mathbf{x}^{(m)}$, it is possible to integrate the various integrands in (3.1) analytically over this small neighbourhood, thereby obtaining the results summarized in appendix B. The neighbourhood is chosen such that, in terms of the local polar co-ordinate system, it is a square of side 2ϵ. For the numerical experiments, the results were insensitive to ϵ for ϵ between 0·01 and 0·20 times the smaller of the two sides of the rectangle Δ_m.

For axisymmetric flow (with the 1 direction taken as the axis of symmetry) past a body which is strictly convex, (2.14) may be used directly since the conditions required for its validity are satisfied. On the other hand, if, as in the case of a finite cylinder with axis in the 1 direction, $R(y_1)$ is not single valued, the

surface integral in (2.11) is first split into domains of constant y_1 and domains where $R(y_1)$ is single valued; the integration in the azimuthal direction is then performed analytically, and the surface integrals are thereby reduced to line integrals over y_1 and y_r. In either case, after dividing the resulting integral(s) to form the elements Δ_m, the integrals over Δ_m are calculated using an adaptive quadrature scheme (a scheme which systematically divides the integration interval into successively smaller subintervals until successive approximations to the integral differ by less than a specified allowable error) based on Simpson's rule with a Richardson extrapolation. The maximum allowable relative error is normally chosen as 10^{-4} or 10^{-5}. In the case of (2.14) it can be shown that the term in the first integrand involving $F(k)$ in the equation for W_1 and the term in the second integrand involving $F(k)$ in the homogeneous equation both become logarithmically infinite as $\mathbf{y} \to \mathbf{x}^{(m)}$. These terms were handled by expanding $F(k)$ for $k \to 1$ and then performing an analytical integration over a small neighbourhood of $\mathbf{x}^{(m)}$ defined typically by $r_{x^{(m)}y}$ less than or equal to 10^{-4} times the characteristic dimension of Δ_m. The remaining integrands all have finite limits as $\mathbf{y} \to \mathbf{x}^{(m)}$ and thus their evaluation presents no difficulties.

The linear algebraic system, which is normally completely dense, was solved using standard Gaussian elimination followed by iterative improvement. The fact that (2.9) has a unique solution suggests, though it does not guarantee, that its discrete approximation, the algebraic system, should also have a unique solution. In fact, for all bodies investigated, the system did have a unique solution. In general, because of the singularity in the corresponding integrand, the diagonal terms are the largest in any row (or column) though not sufficiently large to make the matrix diagonally dominant. Since for large values of N a considerable part, or even the major part, of the computer time is spent inverting (or effectively inverting) the matrix $\{A_{ik}^{(j)}\}$, it is worthwhile to note that since the matrix is a function of only the body geometry and not of the velocity field at infinity [which affects only $g_i(\mathbf{x}^{(m)})$ in (3.1)], it is only necessary to invert it once for all external flows past a given body. In fact, once $\{A_{ik}^{(j)}\}^{-1}$ is known for a certain body, it is a simple matter to obtain the six solutions corresponding to pure translation along and pure rotation about each of the axes of the body and then employ the method of Brenner (1966) to calculate the complete translational and rotational symbolic resistances of the body and thus the net force and torque on the body in an arbitrary Stokes flow.

An inherent difficulty in the numerical solution of integral equations of the first kind is that the problem is well known to be ill conditioned, in the sense that small errors in either $g_i(\mathbf{x}^{(m)})$ or $A_{ik}^{(j)}$ can often produce relatively large errors in f_i. However, as the results in the following section indicate, very accurate solutions were obtained with minimal difficulty, a fact which suggests that any ill conditioning that may exist is much less serious for these particular equations than for other integral equations of the first kind.

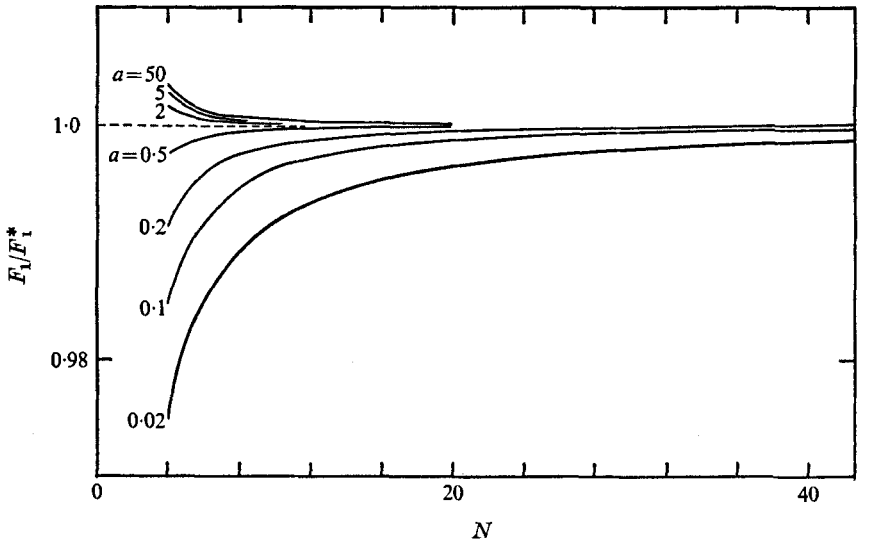

FIGURE 2. Ratio of numerically calculated and analytic drags for spheroids $x_1^2+(x_2^2+x_3^2)/a^2 = 1$ in axisymmetric flow with N equally spaced points.

4. Results

Axisymmetric flows

For any axisymmetric flow, the only parameters in the numerical solution are the number of points N at which the integral equations will be applied and the locations $\mathbf{x}^{(m)}$ of these points. In order to isolate clearly the effect of N, the non-optimal strategy of equal spacing (in the 1 direction) for the $\mathbf{x}^{(m)}$, which makes the solution a function of N only, was applied to the problem of a spheroid given by $x_1^2+(x_2^2+x_3^2)/a^2 = 1$ translating in the 1 direction. A comparison of the numerical drag F_1 with the analytic drag F_1^* (analytic solutions will henceforth be denoted by an asterisk) is shown in figure 2, from which it can be seen that, for spheroids with axis ratios between 0·02 and 50·0, the error in the drag is less than 1 % for $N \geqslant 10$. For a sphere, any choice of N results in essentially no error, which might be expected since f_i^* is constant in this case. The error is greatest for very slender prolate spheroids, for which, as explained below, the policy of spacing the points $\mathbf{x}^{(m)}$ at equal intervals is a poor one.

A more critical evaluation of the numerical method is provided by a comparison of the numerically calculated local stress force with its analytic counterpart. This is effected in figures 3(*a*) and (*b*), where it is evident that the greatest errors in f_1 occur, as expected, in regions where the gradient of f_1 is the largest (f_r^* is identically zero and f_r is zero to the accuracy of the calculations). Figures 4(*a*) and (*b*) indicate that the average (over N) local error decreases rapidly with increasing N, while figures 5(*a*) and (*b*) give the maximum local error as a function of N. The initially surprising result that the maximum error in f_1 for slender prolate spheroids increases with N up to a certain point before starting to decrease results from the policy of equally spacing the points $\mathbf{x}^{(m)}$. That is, for

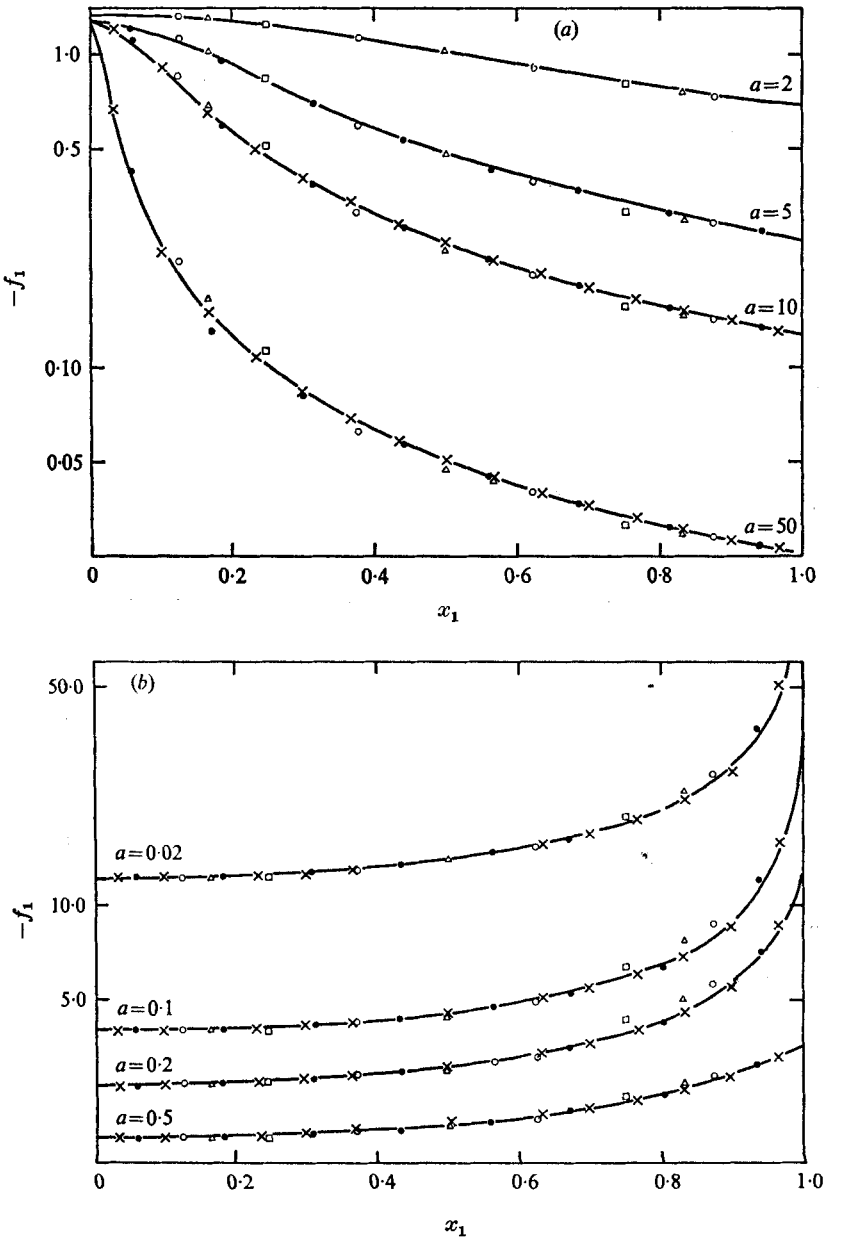

FIGURE 3. Numerically calculated stress force for (*a*) oblate and (*b*) prolate spheroids in axisymmetric flow. □, $N = 4$; △, $N = 6$; ○, $N = 8$; ●, $N = 16$; ×, $N = 30$; ———, analytic solution.

slender prolate spheroids, the gradient in f_1^* is very large near $x_1 = \pm 1{\cdot}0$ [in fact, $f_1^*(x_1 = \pm 1{\cdot}0) = O((a^2 \ln a)^{-1})$ as $a \to 0$], and thus, as the number of equally spaced points along the axis is increased, those near $x_1 = \pm 1{\cdot}0$ move into a region of larger gradient in f_1, with a resultant increase in error. When N becomes sufficiently large, however, the maximum local error starts to decrease

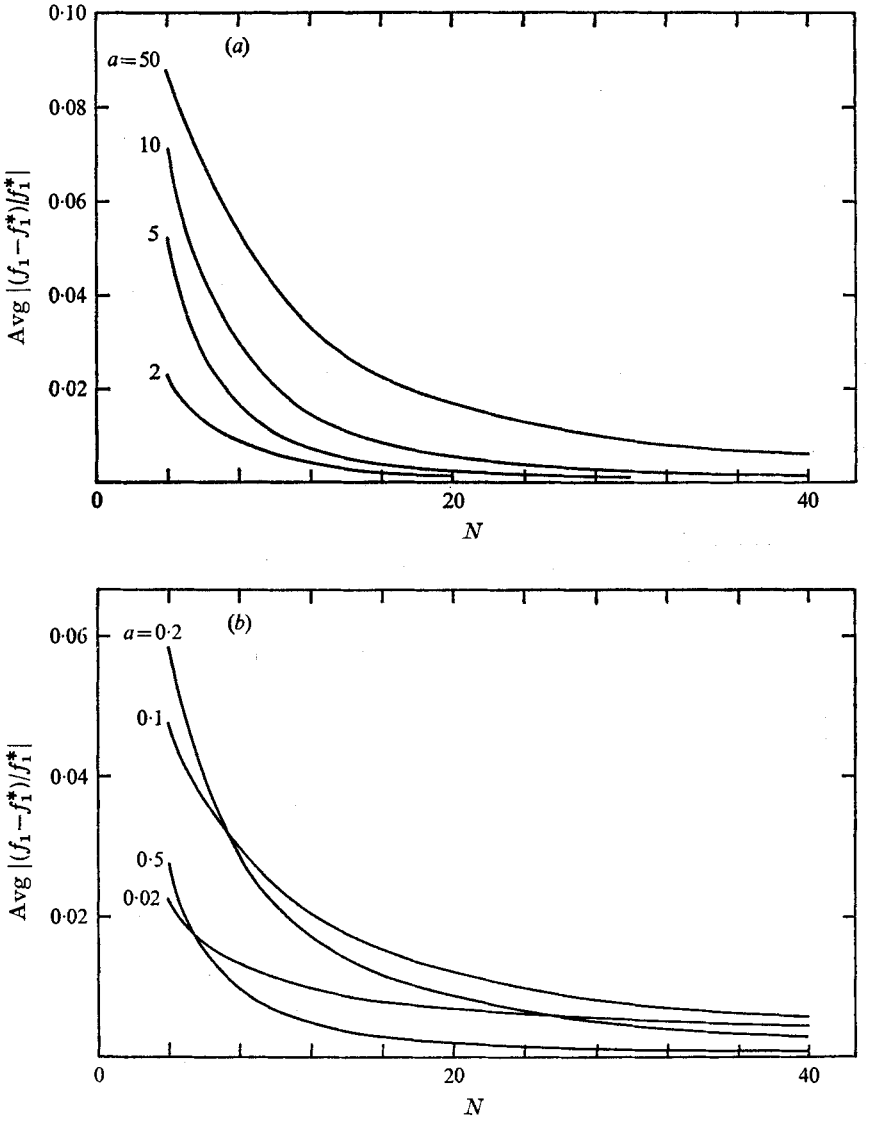

FIGURE 4. Average relative error in stress force for (*a*) oblate and (*b*) prolate spheroids in axisymmetric flow with N equally spaced points.

with increasing N (numerical experiments indicate that for $a = 0{\cdot}02$ the maximum relative error in f_1 would increase to a value of approximately 0·08 at an N of 120 before starting to decrease).

These results seem to suggest that the points $\mathbf{x}^{(m)}$ should be concentrated in regions where the gradients of f_i are the greatest, i.e. near the ends for prolate spheroids. This idea was tested by dividing a prolate spheroid of axis ratio 0·10 into N equal segments as before and then inserting one additional point at each end between the two points nearest the end. This policy, though certainly not optimal, results in the improvements shown in figures 6(*a*) and (*b*). It is

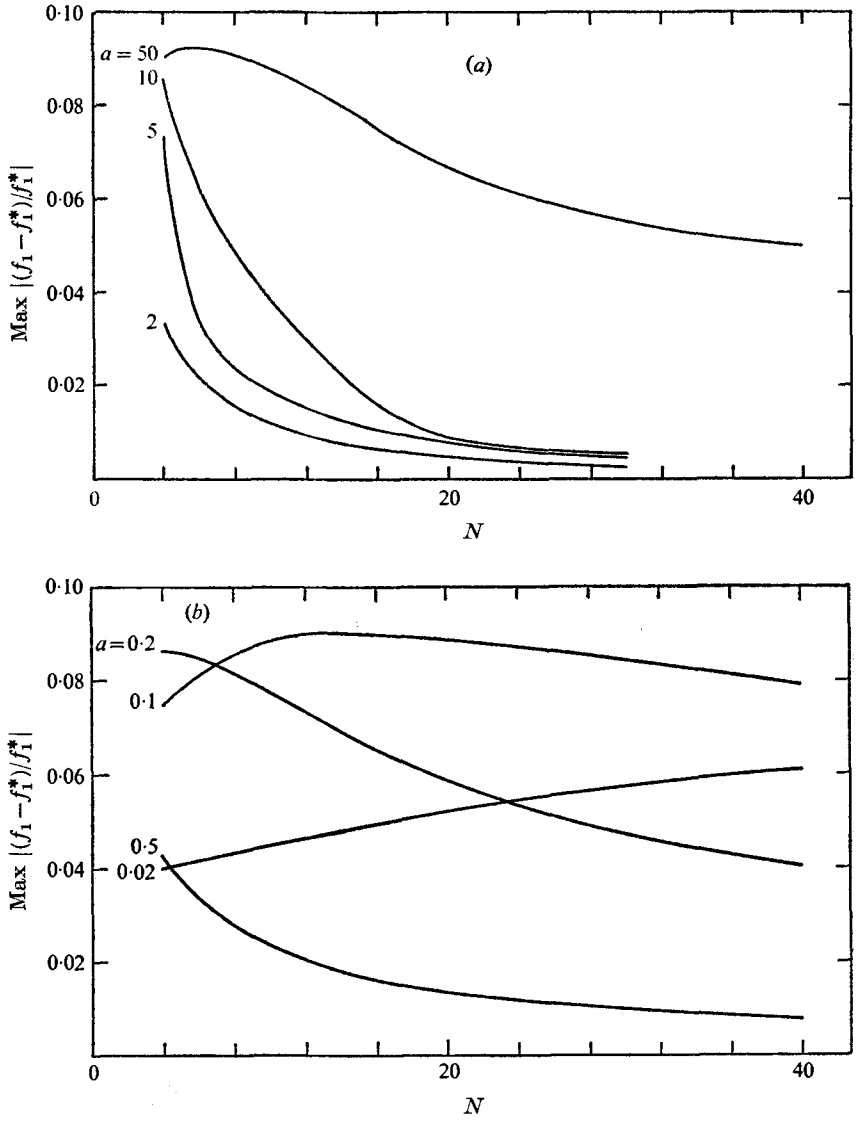

FIGURE 5. Maximum relative error in stress force for (*a*) oblate and (*b*) prolate spheroids in axisymmetric flow with N equally spaced points.

logical to expect, and this was confirmed by experiment, that by concentrating even more points near the ends the error could be reduced still further. For example, using 40 points for $a = 0{\cdot}1$, the largest relative error in f_1 could be made less than 0·01.

Numerical experiments were also performed for axisymmetric flow parallel to the axis of a finite cylinder. In this case, since $R(y_1)$ is not single valued, (2.14) no longer applies but rather must be replaced by its analogue obtained from (2.11) following the procedure outlined in the previous section. Neither the vertical faces at the ends of the cylinder nor the corners of the cylinder caused any difficulty as long as none of the $\mathbf{x}^{(m)}$ were located on the corner. Gluckman

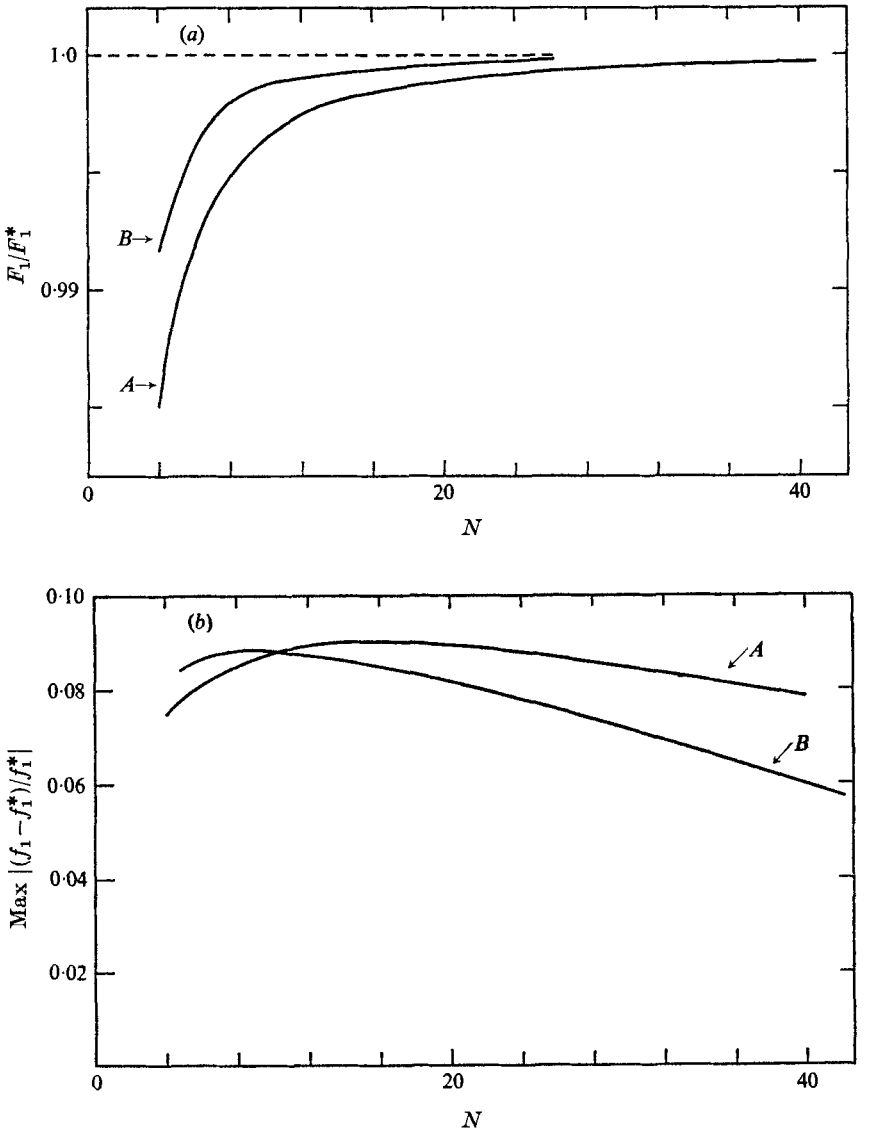

FIGURE 6. (*a*) Ratio of numerically calculated and analytic drags and (*b*) maximum relative error in stress force for two different policies for forming the surface elements. $a = 0{\cdot}1$. *A*, equally spaced elements; *B*, one additional point near each end, otherwise equally spaced elements.

et al. also obtained numerical solutions to this particular problem, though their method, in order to achieve good accuracy, requires that any vertical surfaces be treated differently from non-vertical surfaces. Also their method had to be modified for cylinders of aspect ratio $\geqslant 10$, and even then it did not lead to convergence. As in Gluckman *et al.* the dimensionless drag K on a cylinder is defined as the ratio of the terminal settling velocity of the cylinder to that of a sphere with the same volume as the cylinder or, equivalently, as the ratio of

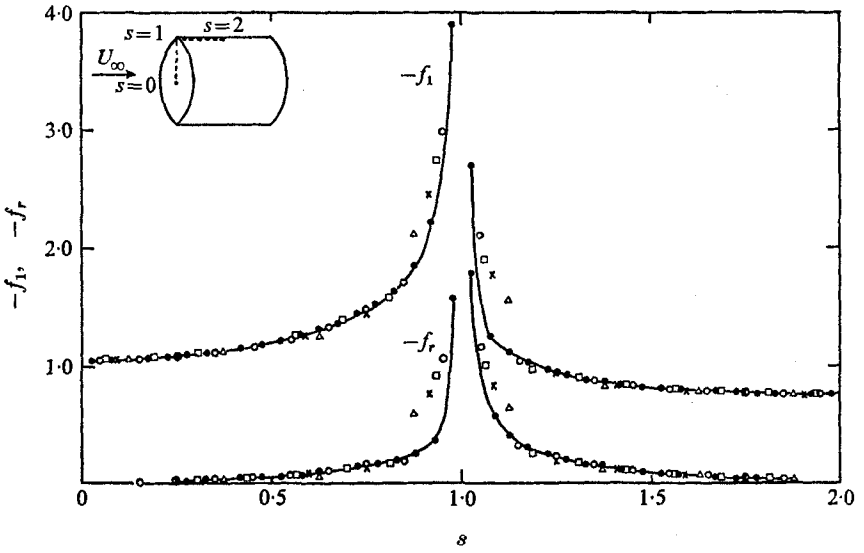

FIGURE 7. Stress force for a cylinder (L/D = 1·0) with N points equally spaced along perimeter. △, N = 16; ×, N = 24; □, N = 32; ○, N = 40; ●, N = 80; —, numerical solution with N = 80 but collocation points concentrated near s = 1.

the drag on a sphere with the same volume as the cylinder to that on the cylinder when both are exposed to the same uniform external flow. Thus

$$K = 6\pi r_s W_1/F_1(\text{cylinder}), \tag{4.1}$$

where $r_s = (\frac{3}{16}LD^2)^{\frac{1}{3}}$ is the radius of the sphere and L and D are the length and diameter of the cylinder. As might be expected in view of the discontinuities in n_i at the corner, $\mathbf{f}$ is, as shown in figure 7, a sensitive function of position near the corner. As a result, a policy of spacing the $\mathbf{x}^{(m)}$ at equal intervals along the perimeter is rather inefficient, and experiments show that increased accuracy can be achieved by concentrating the points near the corner. Table 1 gives K for additional aspect ratios and shows good agreement of the results with those of Gluckman *et al.* Also compared in table 1 are the present results and those obtained by Batchelor (1970),

$$K' = (1{\cdot}5)^{\frac{1}{3}}\left[\ln\frac{L}{D} - 0{\cdot}114 - 0{\cdot}178\left(\ln\frac{L}{D}\right)^{-1} + O\left(\ln\frac{L}{D}\right)^{-2}\right]\left(\frac{D}{L}\right)^{\frac{2}{3}}, \tag{4.2}$$

using slender-body theory. In all cases, the difference between K and K' is of the same order as the error in (4.2).

Three-dimensional flows

The three-dimensional problem is, of course, much more formidable computationally since a two-dimensional integral equation must be solved. *A priori* it might be expected that, if N points are required for a certain accuracy in the axisymmetric case, approximately N^2 points would be required to achieve comparable accuracy in the three-dimensional case. Since 20 might be considered a typical value of N for axisymmetric flows, this would indicate that an N of

Aspect ratio L/D	Number of surface elements, N	Numerical drag K	Gluckman *et al.*† $K_G(N_{ps})$	K'
0·5	8	0·879	0·877	—
	16	0·875		
	24	0·873		
	32	0·873		
1·0	8	0·962	0·960	
	16	0·956		
	24	0·955		
	32	0·954		
	40	0·954		
2·0	8	0·986	0·986	—
	16	0·980		
	24	0·978		
	32	0·977		
	40	0·977		
4·0	8	0·938	0·929	—
	16	0·934		
	24	0·932		
	32	0·932		
10·0	8	0·794	0·932 (1)	0·781
	16	0·789	0·876 (2)	
	24	0·788	0·855 (3)	
	32	0·788	0·837 (5)	
20·0	8	0·659	0·695 (3)	0·658
	16	0·650	0·683 (5)	
	24	0·649	0·674 (9)	
	32	0·649	0·668 (15)	
40·0	8	0·528	0·539 (3)	0·518
	16	0·513	0·531 (5)	
	24	0·510	0·525 (9)	
	32	0·510	0·522 (15)	
60·0	8	0·455		0·441
	16	0·438		
	24	0·436		
	32	0·435		
	40	0·435		
80·0	8	0·404		0·391
	16	0·390		
	24	0·387		
	32	0·387		
100·0	8	0·365		0·354
	16	0·354		
	24	0·352		
	32	0·351		
	40	0·351		

† For $10 \leqslant L/D \leqslant 40$, N_{ps} is the number of touching prolate spheroidal singularities used by Gluckman *et al.* to approximate the cylinder.

TABLE 1. Drag results for finite cylinders. The collocation points $\mathbf{x}^{(m)}$ were distributed non-uniformly with $|\mathbf{x}^{(m-1)} - \mathbf{x}^{(m)}| \approx |\mathbf{x}^{(m)} - \mathbf{x}^{(m+1)}|$ but such that the distance between the collocation points at the centre of the cylinder was approximately 10 times the distance between the collocation points near the corners.

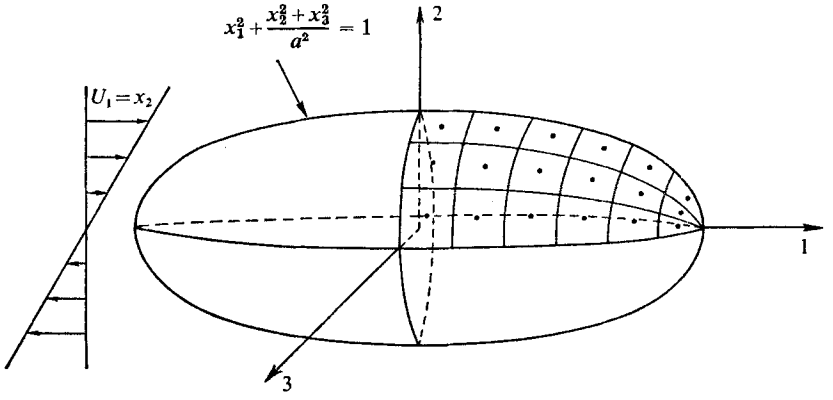

FIGURE 8. Simple shear flow past a prolate spheroid divided into 144 elements with $\eta_x = 6$, $\eta_\theta = 3$.

400 might be typical in three dimensions. This would lead to 1200 algebraic equations, which in general would have to be solved directly. This, computationally, would be such a formidable task that smaller values of N would have to be used, leading to an expected attendant decrease in accuracy. However, as will be seen, the loss of accuracy is in many cases relatively slight and not nearly as large as might first be expected.

Because the use of an adaptive quadrature scheme is inherently inefficient and since the calculation of the double integrals in (3.1) constitutes a significant portion of the total computer time for most three-dimensional problems, a simple product Gaussian rule, rather than an adaptive rule as was used in the axisymmetric case, was employed to calculate the coefficients in the algebraic system. Thus, the results in any three-dimensional problem depend on the particular integration rule that is being used as well as on the number of elements into which the body is divided and on the geometry of these elements. In addition, because of the extra dimension, the dependence on the manner of forming the N elements is more complex in three dimensions that in two. Specifically, unlike the axisymmetric case, no simple policy for forming the Δ_m could be found that rendered the solution a unique function of N. For example, if a simple body such as a sphere in a simple shear is divided into N elements, then merely rotating the lines dividing the Δ_m by a fixed amount will, in general, yield slightly different results.

Numerical experiments were conducted on a prolate spheroid

$$x_1^2+(x_2^2+x_3^2)/a^2 = 1$$

with $U_i(\mathbf{x}) = \delta_{i1}x_2$, which corresponds to a stationary prolate spheroid placed symmetrically in a simple shear flow parallel to its major axis. As shown in figure 8, the spheroid was divided into $N = 8\eta_x\eta_\theta$ elements by first using the planes $x_1 = 0$, $x_2 = 0$ and $x_3 = 0$ to form eight symmetric regions, each of which was subsequently divided to form the elements Δ_m by spacing the $\mathbf{x}^{(m)}$ at η_x equal intervals in the 1 direction and at η_θ equal intervals with respect to the azimuthal angle θ.

a	η_x	η_θ	N	Couple ratio T_3/T_3^*	Max $\lvert\lvert\mathbf{f}\rvert-\lvert\mathbf{f}^*\rvert\rvert$	Max $\left\lvert\frac{\lvert\mathbf{f}\rvert-\lvert\mathbf{f}^*\rvert}{\lvert\mathbf{f}^*\rvert}\right\rvert$	Max $\lvert f_1-f_1^*\rvert$	Max $\left\lvert\frac{f_1-f_1^*}{f_1^*}\right\rvert$	Max $\lvert f_2-f_2^*\rvert$	Max $\left\lvert\frac{f_2-f_2^*}{f_2^*}\right\rvert$	Avg $\left\lvert\frac{f_1-f_1^*}{f_1^*}\right\rvert$	Avg $\left\lvert\frac{f_2-f_2^*}{f_2^*}\right\rvert$
1·0	1	1	8	0·9457	0·0004	0·0002	0·0004	0·0002	0·0541	†	0·0002	0·0541‡
	2	1	16	0·9506	0·0746	0·0363	0·0741	0·0361	0·0515		0·0238	0·0491
	4	2	64	0·9971	0·0904	0·0328	0·0904	0·0329	0·0280		0·0190	0·0141
	6	3	144	1·0010	0·0682	0·0277	0·0682	0·0289	0·0154		0·0155	0·0048
0·5	1	1	8	0·9647	0·0204	0·0160	0·0204	0·0160	0·0228	1·4008	0·0161	1·4008
	2	1	16	0·9575	0·0384	0·0294	0·0384	0·0294	0·0277	1·0907	0·0258	1·0671
	4	2	64	0·9952	0·0407	0·0254	0·0406	0·0254	0·0368	0·9336	0·0156	0·4611
	6	3	144	0·9988	0·0291	0·0312	0·0291	0·0236	0·0255	0·5753	0·0122	0·1182
0·2	1	1	8	1·0028	0·0212	0·0240	0·0213	0·0240	0·0041	0·1912	0·0241	0·1912
	2	1	16	0·9787	0·0283	0·0324	0·0286	0·0330	0·0093	0·2440	0·0324	0·2349
	4	2	64	1·0006	0·0199	0·0171	0·0199	0·0171	0·0195	0·3054	0·0140	0·1390
	6	3	144	1·0006	0·0106	0·0265	0·0107	0·0106	0·0256	0·3267	0·0082	0·0528
0·1	1	1	8	1·0806	0·0275	0·0356	0·0276	0·0356	0·0011	0·0642	0·0356	0·0642
	2	1	16	1·0107	0·0323	0·0419	0·0324	0·0421	0·0032	0·1552	0·0418	0·1262
	4	2	64	1·0131	0·0196	0·0194	0·0196	0·0194	0·0086	0·1598	0·0165	0·0668
	6	3	144	1·0077	0·0101	0·0097	0·0101	0·0097	0·0127	0·1891	0·0074	0·0275
0·05	1	1	8	1·0496	0·0755	0·1035	0·0755	0·1034	0·0028	0·2483	0·1034	0·2483
	2	1	16	0·9770	0·0403	0·0552	0·0403	0·0552	0·0030	0·3227	0·0309	0·2282
	4	2	64	1·0061	0·0138	0·0151	0·0139	0·0147	0·0072	0·3188	0·0053	0·1903
	6	3	144	1·0033	0·0112	0·0130	0·0114	0·0116	0·0082	0·1838	0·0046	0·0640
0·02	1	1	8	1·2932	0·0360	0·0506	0·0360	0·0506	0·0014	0·2306	0·0506	0·2306
	2	1	16	1·0718	0·1582	0·2222	0·1582	0·2221	0·0054	0·4624	0·1798	0·4115
	8	1	64	0·9649	0·0280	0·0393	0·0280	0·0392	0·0035	0·1279	0·0293	0·0762
	18	1	144	0·9735	0·0311	0·0436	0·0310	0·0436	0·0031	0·0932	0·0400	0·0856

† For a sphere, $f_2^* \equiv 0$; thus relative error is not defined.
‡ Average absolute error, rather than relative error.

TABLE 2. Results for simple shear flow past prolate spheroids

a	η_x	η_θ	N	Couple ratio T_3/T_3^*	Max $\lvert\lvert\mathbf{f}\rvert-\lvert\mathbf{f}^*\rvert\rvert$	Max $\left\lvert\frac{\lvert\mathbf{f}\rvert-\lvert\mathbf{f}^*\rvert}{\lvert\mathbf{f}^*\rvert}\right\rvert$	Max $\lvert f_1-f_1^*\rvert$	Max $\left\lvert\frac{f_1-f_1^*}{f_1^*}\right\rvert$	Max $\lvert f_2-f_2^*\rvert$	Max $\left\lvert\frac{f_2-f_2^*}{f_2^*}\right\rvert$	Avg $\left\lvert\frac{f_1-f_1^*}{f_1^*}\right\rvert$	Avg $\left\lvert\frac{f_2-f_2^*}{f_2^*}\right\rvert$
1·0	2	1	16	0·9506	0·0746	0·0363	0·0741	0·0361	0·0515	†	0·0238	0·0491‡
	4	2	64	0·9971	0·0502	0·0328	0·0502	0·0329	0·0280		0·0190	0·0141
	6	3	144	1·0010	0·0506	0·0277	0·0506	0·0289	0·0154		0·0155	0·0048
1·0	2	2	32	0·9990	0·0974	0·0363	0·0974	0·0363	0·0500	†	0·0226	0·0242‡
	3	3	72	1·0015	0·0684	0·0298	0·0684	0·0323	0·0299		0·0230	0·0076
	4	4	128	1·0016	0·0449	0·0360	0·0450	0·0387	0·0220		0·0190	0·0049
						Using 3 × 8 *product Gaussian integration formula*						
0·1	1	1	8	1·0806	0·0275	0·0356	0·0276	0·0356	0·0011	0·0642	0·0356	0·0642
	2	1	16	1·0107	0·0323	0·0419	0·0324	0·0421	0·0032	0·1552	0·0418	0·1262
	4	2	64	1·0131	0·0196	0·0194	0·0196	0·0194	0·0086	0·1598	0·0165	0·0668
	6	3	144	1·0077	0·0101	0·0097	0·0101	0·0097	0·0127	0·1891	0·0074	0·0275
						Using 4 × 4 *product Gaussian integration formula*						
0·1	1	1	8	0·9715	0·0720	0·0930	0·0719	0·0930	0·0051	0·2943	0·0930	0·2943
	2	1	16	0·9533	0·0352	0·0454	0·0351	0·0453	0·0059	0·3910	0·0262	0·2834
	4	2	64	0·9924	0·0129	0·0128	0·0132	0·0136	0·0171	0·3718	0·0056	0·2456
	6	3	144	0·9951	0·0104	0·0235	0·0107	0·0110	0·0202	0·3009	0·0047	0·0888

† For a sphere, $f_2^* = 0$; thus relative error is undefined.
‡ Average absolute error, rather than relative error.

TABLE 3. Effect of η_x and η_θ on results for a sphere and effect of integration formula for spheroid with $a = 0{\cdot}1$

The two-dimensional integration formula which is most appropriate for a given problem depends on the shape of the Δ_m. For elements which are approximately square in terms of the x_1, θ cylindrical co-ordinates used, symmetric product rules would appear to be most appropriate. In the present numerical experiments, symmetric product Gaussian rules constructed from either four- or eight-point one-dimensional formulae, thus using 16 and 64 points respectively, were employed for spheroids with $0{\cdot}2 \leqslant a \leqslant 1{\cdot}0$, while for the more elongated elements associated with spheroids with axis ratios between 0·02 and 0·10, either 3×8 or 4×16 product Gaussian formulae were used. In all the experiments, the high-order formula in any pair was employed on the element containing the singularity and the low-order formula for the remaining integrals.

Table 2 summarizes the results for the three-dimensional experiments and shows that the couple T_3 normally had an error of approximately 1 % or less. The analytic total force F_i^* on the particle is, of course, identically zero and, indeed, the numerical total force F_i was found to be zero to machine accuracy. Also the largest relative errors in $|\mathbf{f}|$ and f_1 were normally less than 5 % with an average relative error of about 1 %. However, since f_2 is typically one or two orders of magnitude smaller than f_1, while its absolute error is normally comparable with or less than the absolute error in f_1, its relative error was naturally somewhat larger. But, as may be seen by comparing the errors in $|\mathbf{f}|$ and f_1, the errors in f_2 have a very slight effect on errors in the local stress force $\mathbf{f}$.

Table 3 summarizes two experiments which demonstrate the relative insensitivity of the results to the manner in which the elements Δ_m were formed and to the particular integration formula used. In the first experiment, which was intended to consider the effect of element shape, the surface elements of a sphere were constructed in two different ways: $\eta_x = 2\eta_\theta (\eta_\theta = 1, 2, 3)$ and $\eta_x = \eta_\theta$ $(\eta_\theta = 2, 3, 4)$. As can be seen, the results are nearly identical. The second experiment used the same elements on a spheroid with $a = 0{\cdot}1$ but employed one of two different integration formulae: either a 3×8 or a 4×4 product Gaussian rule. Again the results are very similar, with, as might be expected, the 3×8 formula being slightly superior. However, for more elongated spheroids the 3×8 formula is definitely more accurate and in the case $a = 0{\cdot}05$ gives errors which are roughly half as large as those resulting from use of the 4×4 formula. It was also found that, for $0{\cdot}1 \leqslant a \leqslant 1{\cdot}0$, the results were insensitive to the element shape for elements whose length-to-height ratio was between 0·1 and 10·0, and that, for these element shapes, it made little difference whether the 4×4 or the 3×8 integration formula was employed.

A three-dimensional problem of practical significance, owing to its occurrence in nature and its suitability for experimental investigation, is that of determining the angular velocity of a finite circular cylinder freely suspended in a general linear shear flow. As has been demonstrated experimentally (Goldsmith & Mason 1967) and theoretically (Brenner 1964*b*), the expression for the angular velocity contains a single unknown scalar, the equivalent axis ratio r_e, defined as the axis ratio of that spheroid which would, when freely suspended in the same flow field at infinity, experience the same periodic motion as the cylinder. Unfortunately, if the cylinder has length L and diameter D, the determination

$\frac{L}{D}$	N	$\frac{r_e}{L/D}$	T_3'/L^3	T_c'/L^3	T_3''/L^3	$\frac{8T''_{\text{end}}}{LD^2}$	$\frac{4T''_{\text{side}} \ln L/D}{\pi LD^2}$
1·00	144	1·16	26·6	∞	19·8	8·3	0
	112	1·15	26·4		20·1		
	80	1·13	25·9		20·2		
	40	1·12	25·0		20·0		
1·67	144	1·02	16·3	31·7	5·60	5·1	0·85
	112	1·02	16·2		5·61		
	80	1·01	15·9		5·57		
	40	1·02	15·9		5·53		
2·50	144	0·939	11·6	13·9	2·09	3·8	1·4
	112	0·938	11·5		2·09		
	80	0·938	11·3		2·06		
	40	0·928	11·3		2·11		
10·0	144	0·749	4·74	4·39	$8{\cdot}4 \times 10^{-2}$	2·8	2·1
	112	0·748	4·72		8·4		
	80	0·745	4·70		8·5		
	40	0·726	4·66		8·9		
16·7	144	0·702	3·73	3·48	$2{\cdot}7 \times 10^{-2}$	2·7	2·2
	112	0·700	3·71		2·7		
	80	0·694	3·67		2·7		
	40	0·673	3·65		2·9		
25·0	144	0·657	3·19	2·99	$1{\cdot}2 \times 10^{-2}$	2·8	2·3
	112	0·657	3·18		1·2		
	80	0·655	3·17		1·2		
	40	0·661	3·11		1·1		
50·0	144	0·612	2·52	2·40	$2{\cdot}7 \times 10^{-3}$	2·7	2·5
	112	0·611	2·51		2·7		
	80	0·605	2·50		2·7		
	40	0·621	2·48		2·6		
100·0	144	0·574	2·07	2·01	$6{\cdot}3 \times 10^{-4}$	2·8	2·6
	112	0·573	2·07		6·3		
	80	0·575	2·08		6·3		
	40	0·564	2·16		6·8		
166·7	144	0·555	1·84	1·79	$2{\cdot}1 \times 10^{-4}$	2·9	2·5
	112	0·560	1·86		2·1		
	80	0·570	1·88		2·1		
	40	0·568	1·88		2·1		

TABLE 4. Equivalent axis ratios of circular cylinders

of r_e is analytically intractable for $L/D = O(1)$; furthermore, as discussed by Cox (1971), the problem cannot be solved completely using slender-body theory when $L/D \gg 1$, owing to the presence of the blunt ends of the cylinder. Cox (1971) has shown, however, that r_e is given by

$$r_e = (T_3'/T_3'')^{\frac{1}{3}}, \tag{4.3}$$

where T_3' and T_3'' are, respectively, the torques experienced by a stationary cylinder centred at the origin with axis in the 1 direction when exposed to simple shear flows at infinity given by

$$U_i' = -\delta_{i2}x_1, \quad U_i'' = \delta_{i1}x_2. \tag{4.4a, b}$$

The problem (2.1) with (4.4) was solved numerically using the same integration methods and the same procedure for constructing the surface elements as in the previous example. The results are shown in figure 9, where they are compared with the available experimental data. Clearly, the agreement with experiment is very good for $L/D \leqslant 100$, but for $L/D > 100$, r_e does not fall as rapidly with increasing L/D as the recent experimental data of Harris & Pittman (1975).

The numerical solution definitely becomes more difficult at very large L/D, for at least two reasons. First, as seen in all the previous solutions, numerical errors increase as the elements Δ_m become more elongated. Second, the evaluation of T_3'' is subject to more errors because the contribution to T_3'' from the forces acting near the corners of the cylinder becomes relatively more important as L/D increases, and the calculation of these forces is, for all aspect ratios, the most difficult, and hence the most error prone part of the computations. Nevertheless, the numerical results appear reliable because of their excellent agreement with the experimental data of Anczurowski & Mason (1968) and the fact that, as will be seen below, they are entirely consistent with the slender-body analysis of Cox. It is felt, therefore, that the findings of Harris & Pittman, especially at larger values of L/D, should be looked at anew.

Table 4 summarizes the numerical results and compares T_3' with the value given by slender-body theory (Cox 1971):

$$T_c' = \frac{\pi L^3}{3}\left[\frac{1}{\ln L/D} + \frac{0{\cdot}447}{(\ln L/D)^2} + O\left(\ln\frac{L}{D}\right)^{-3}\right]. \tag{4.5}$$

In all cases, T_3' and T_c' agree to $O[(\ln L/D)^{-3}]$. In fact, if T_c' is written to higher order as

$$T_c' = \frac{\pi L^3}{3}\left[\frac{1}{\ln L/D} + \frac{0{\cdot}447}{(\ln L/D)^2} + \frac{0{\cdot}10}{(\ln L/D)^3} + O\left(\ln\frac{L}{D}\right)^{-4}\right], \tag{4.6}$$

agreement to three significant figures is obtained for $L/D \geqslant 25$.

The slender-body analysis of Cox (1971) cannot determine T_3'' quantitatively for blunt bodies since it is unable to handle properly the ends of the cylinder, which make a major contribution to the torque. Cox observes that, for large L/D, T_3'' is equal to the torque T_{end}'' due to forces acting on the ends, i.e.

$$T_3'' \approx T_{\text{end}}'' = \tfrac{1}{8}\alpha_c L D^2, \tag{4.7}$$

where α_c is a constant, whose value Cox estimated to be 5·45 by using (4.3), (4.5) and (4.7) and fitting the experimental data of Anczurowski & Mason (1968). On a strictly empirical basis, Harris & Pittman (1975) later proposed that

$$T_3'' = \frac{\alpha_H}{8} L D^2\left[1 + \frac{K_H}{\ln 2L/D}\right], \tag{4.8}$$

and determined the constants $\alpha_H = 9{\cdot}0$ and $K_H = -1{\cdot}21$ from their experimental data and those of Anczurowski & Mason.

However, if T_3'' is decomposed into

$$T_3'' = T_{\text{end}}'' + T_{\text{side}}'', \tag{4.9}$$

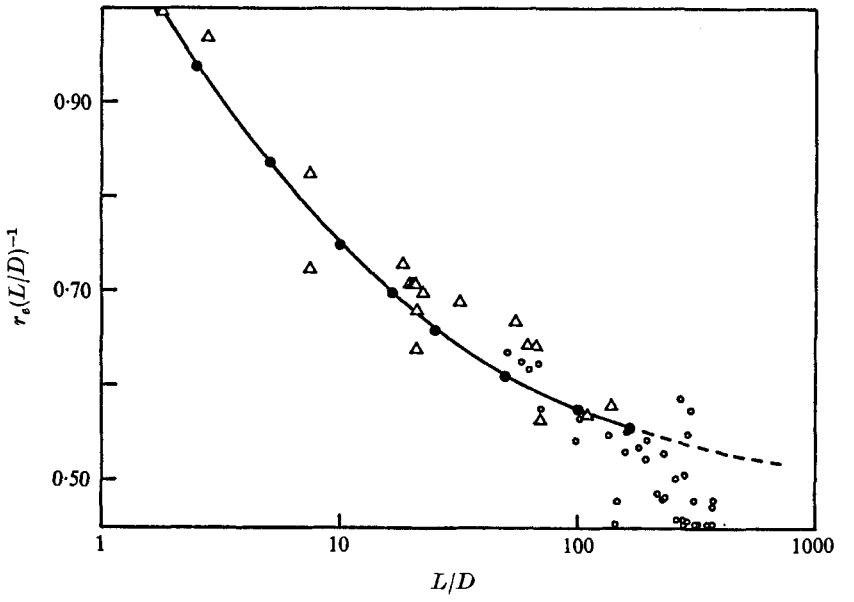

FIGURE 9. Equivalent axis ratio of circular cylinders. △, Anczurowski & Mason (1968); ○, Harris & Pittman (1975); —●—, numerical results; — — —, equation (4.12).

where T''_{side} is the contribution to the torque of the forces acting on the sides of cylinder, Cox's analysis indicates that

$$T''_{\text{end}} = \frac{k_1}{8} LD^2, \quad T''_{\text{side}} = \frac{\pi k_2 LD^2}{4 \ln L/D} + O\left[\left(\ln \frac{L}{D}\right)^{-2}\right], \tag{4.10}$$

where the constants k_1 and k_2 can be independently determined from the numerical results. As seen in table 4, k_1 and k_2 are 2·8 and 2·6 respectively with an error estimated to be less than 4%. Therefore

$$T''_3 = 0{\cdot}35 LD^2 \left[1 + \frac{5{\cdot}8}{\ln L/D}\right], \tag{4.11}$$

which is of the same form as the expression proposed empirically by Harris & Pittman. However, since (4.8) should be viewed as the sum of T''_{end} and T''_{side}, α_H and K_H are necessarily positive, in contrast to Harris & Pittman's empirical result $K_H = -1{\cdot}21$. On the other hand, the large discrepancy between the values $k_1 = 2{\cdot}8$ and $\alpha_c = 5{\cdot}45$ proposed by Cox is due to the fact that at the largest aspect ratio studied by Anczurowski & Mason (≈ 100), T''_{end} and T''_{side} are, according to the present calculations, still of the same order of magnitude, and thus the assumption $T''_3 \approx T''_{\text{end}}$ is invalid.

By combining (4.3), (4.5) and (4.11) we therefore obtain, finally,

$$\frac{r_e}{L/D} = \left\{3{\cdot}0 \left(\frac{1}{\ln L/D} + \frac{0{\cdot}447}{(\ln L/D)^2}\right) \Big/ \left(1 + \frac{5{\cdot}8}{\ln L/D}\right)\right\}^{\frac{1}{2}} \tag{4.12}$$

for large L/D. As expected, and as shown in figure 9, equation (4.12) fits the numerical results smoothly and does not fall off as rapidly as the data of Harris & Pittman.

All computations were performed on Stanford's IBM 360/67, and by taking advantage of the symmetry in the three-dimensional problems, no single experiment required more than one minute of computer time. In fact, a typical axisymmetric calculation with 30 points or a three-dimensional experiment with 60 points required approximately 15–20 s.

This work was supported in part by the National Science Foundation under grants GK 41781 and GK 36515X and by an N.S.F. fellowship to G.K.Y. The authors are grateful to Howard Brenner for his helpful suggestions.

Appendix A. Proof that (2.9) has a unique solution

Since, as shown by Odqvist, (2.1) and (2.2) have a solution $\mathbf{v}$, it follows that $f_i = T_{ij}(\mathbf{v})\, n_j$ is a solution of (2.9). To show that this solution is unique it is sufficient to show that the homogeneous equation

$$0 = \frac{1}{8\pi}\iint_{S_p}\left[\frac{\delta_{ik}}{r_{xy}} + \frac{(x_i - y_i)\,(x_k - y_k)}{r_{xy}^3}\right]\phi_i(\mathbf{y})\, dS_y, \quad \mathbf{x} \in S_p, \tag{A 1}$$

has only the trivial solution. Consider the velocity field w_i formed from a solution ϕ_i of (A 1),

$$w_i(\mathbf{x}) \equiv \frac{1}{8\pi}\iint_{S_p}\left[\frac{\delta_{ik}}{r_{xy}} + \frac{(x_i - y_i)\,(x_k - y_k)}{r_{xy}^3}\right]\phi_i(\mathbf{y})\, dS_y, \quad \mathbf{x} \in \Omega, \tag{A 2}$$

and its associated stress field

$$T_{ij}(\mathbf{w}) = \frac{-3}{4\pi}\iint_{S_p}\frac{(x_i - y_i)\,(x_j - y_j)\,(x_k - y_k)\,\phi_k(\mathbf{y})}{r_{xy}^5}\, dS_y, \quad \mathbf{x} \in \Omega, \tag{A 3}$$

which has a jump at S_p given by

$$\lim_{\mathbf{x}\to\mathbf{x}_0} T_{ij}(\mathbf{w}(\mathbf{x}))\, n_j(\mathbf{x}) = \tfrac{1}{2}\phi_i(\mathbf{x}_0) + T_{ij}(\mathbf{w}(\mathbf{x}))|_{\mathbf{x}_0} n_j(\mathbf{x}_0), \quad \mathbf{x} \in \Omega, \quad \mathbf{x}_0 \in S_p. \tag{A 4}$$

Now $w_i(\mathbf{x}) \to 0$ as $\mathbf{x} \to \infty$ and $w_i(\mathbf{x}) = 0$ on S_p by (A 1) since the single-layer potential is continuous at S_p. Therefore, since w_i, together with its associated pressure, which is equal to a single-layer potential with density ϕ_i, satisfies (2.1) and is zero on S_p and at infinity, the uniqueness proof of Odqvist for the Stokes problem implies that $w_i(\mathbf{x})$ and hence $T_{ij}(\mathbf{w})$ must be identically zero everywhere. Thus ϕ_i is also identically zero by (A 4).

Appendix B

We give values of $A_{ik}^{(m)}(\mathbf{x}^{(m)}, \epsilon)$ and $V_i^{(2)}(\mathbf{x}^{(m)}, \epsilon)$ representing those parts of $A_{ik}^{(m)}(\mathbf{x}^{(m)})$ and $V_i^{(2)}(\mathbf{x}^{(m)})$ which result from integration over the planar square S_ϵ centred at $\mathbf{x}^{(m)}$ with sides of length 2ϵ and along lines of constant x_1 and constant θ. To begin with, from (3.1),

$$A_{ik}^{(m)}(\mathbf{x}^{(m)}, \epsilon) \equiv \frac{1}{4\pi}\iint_{S_\epsilon}\left[\frac{\delta_{ik}}{r_{x^{(m)}y}} + \frac{(x_i^{(m)} - y_i)\,(x_k^{(m)} - y_k)}{r_{x^{(m)}y}^3}\right] dS_y. \tag{B 1}$$

Next, if the actual surface of the particle is given by $R(x_1, \theta)$, it can be shown that

$$x_1 - y_1 = \frac{r_{xy}\cos\omega}{(1+R'^2)^{\frac{1}{2}}}, \tag{B 2a}$$

$$x_2 - y_2 = \frac{r_{xy} n_3 \sin\omega}{(n_2^2+n_3^2)^{\frac{1}{2}}} - \frac{r_{xy} n_2 R' \cos\omega}{(n_2^2+n_3^2)^{\frac{1}{2}}(1+R'^2)^{\frac{1}{2}}}, \tag{B 2b}$$

$$x_3 - y_3 = \frac{-r_{xy} n_2 \sin\omega}{(n_2^2+n_3^2)^{\frac{1}{2}}} - \frac{r_{xy} n_3 R' \cos\omega}{(n_2^2+n_3^2)^{\frac{1}{2}}(1+R'^2)^{\frac{1}{2}}}, \tag{B 2c}$$

where $\theta = \tan^{-1} x_2/x_3$, $R' \equiv \partial R/\partial x_1$, all quantities are evaluated at $\mathbf{x}^{(m)}$, and ω is the angle between r_{xy} and the projection of the negative 1 axis onto S_ϵ. When substituted into (B 1), these expressions yield

$$A_{11}^{(m)}(\mathbf{x}^{(m)}, \epsilon) = \frac{\epsilon}{2\pi}\left[\ln\frac{\sqrt{2}+1}{\sqrt{2}-1}\right]\left[2+\frac{1}{1+R'^2}\right]$$

$$= 0{\cdot}2805\epsilon\left[2+\frac{1}{1+R'^2}\right], \tag{B 3}$$

$$A_{12}^{(m)} = \frac{-0{\cdot}2805 n_2 R'\epsilon}{[1+R'^2](n_2^2+n_3^2)^{\frac{1}{2}}}, \quad A_{13}^{(m)} = \frac{-0{\cdot}2805 n_3 R'\epsilon}{[1+R'^2](n_2^2+n_3^2)^{\frac{1}{2}}}, \tag{B 4), (B 5}$$

$$A_{22}^{(m)} = 0{\cdot}2805\epsilon\left[2+\frac{n_3^2+R'^2(n_2^2+n_3^2)}{(n_2^2+n_3^2)\{1+R'^2\}}\right], \tag{B 6}$$

$$A_{23}^{(m)} = \frac{-0{\cdot}2805\epsilon n_2 n_3}{(n_2^2+n_3^2)[1+R'^2]}, \tag{B 7}$$

$$A_{33}^{(m)} = 0{\cdot}2805\epsilon\left[2+\frac{n_2^2+R'^2(n_2^2+n_3^2)}{(n_2^2+n_3^2)\{1+R'^2\}}\right]. \tag{B 8}$$

To calculate $V_k^{(2)}(\mathbf{x}^{(m)}, \epsilon)$, use (2.10) to obtain

$$V_k^{(2)}(\mathbf{x}) = \frac{3}{4\pi}\iint_{S_p} \frac{(x_i-y_i)(x_j-y_j)(x_k-y_k)\, n_j(\mathbf{y})\,[U_i(\mathbf{y})-U_i(\mathbf{x})+U_i(\mathbf{x})]}{r_{xy}^5} dS_y$$

$$= \tfrac{1}{2}U_k(\mathbf{x}) + \frac{3}{4\pi}\iint_{S_p} \frac{(x_i-y_i)(x_j-y_j)(x_k-y_k)\, n_j(\mathbf{y})\,[U_i(\mathbf{y})-U_i(\mathbf{x})]}{r_{xy}^5} dS_y \tag{B 9}$$

$$= \tfrac{1}{2}U_k(\mathbf{x}) + \frac{3}{4\pi}\iint_{S_p - S_\epsilon} \frac{(x_i-y_i)(x_j-y_j)(x_k-y_k)\, n_j(\mathbf{y})\,[U_i(\mathbf{y})-U_i(\mathbf{x})]}{r_{xy}^5} dS_y$$

$$+ \frac{3}{4\pi}\iint_{S_\epsilon} \frac{(x_i-y_i)(x_j-y_j)(x_k-y_k)\, n_j(\mathbf{y})\,[U_i(\mathbf{y})-U_i(\mathbf{x})]}{r_{xy}^5} dS_y. \tag{B 10}$$

Clearly $V_k^{(2)}(\mathbf{x})$ is easily calculated numerically if the integral over S_ϵ can be evaluated. But

$$G_k(\mathbf{x}^{(m)}, \epsilon) \equiv \frac{3}{4\pi}\iint_{S_\epsilon} \frac{(x_i^{(m)}-y_i)(x_j^{(m)}-y_j)(x_k^{(m)}-y_k)\, n_j(\mathbf{y})\,[U_i(\mathbf{y})-U_i(\mathbf{x})]}{r_{x^{(m)}y}^5} dS_y = O(\epsilon) \tag{B 11}$$

and could be neglected to a first approximation. However if $U_i(\mathbf{x}) = C_{ij}x_j$, then the integration in (B 11) can be performed analytically, yielding

$$G_1(\mathbf{x}^{(m)}, \epsilon) = -A_1\epsilon[0{\cdot}6166B_1 + 0{\cdot}2251B_3], \tag{B 12}$$

$$G_2(\mathbf{x}^{(m)}, \epsilon) = -\epsilon[\{0{\cdot}6166B_1 + 0{\cdot}2251B_3\}A_2 + 0{\cdot}2251B_2A_3], \tag{B 13}$$

$$G_3(\mathbf{x}^{(m)}, \epsilon) = -\epsilon[\{0{\cdot}6166B_1 + 0{\cdot}2251B_3\}A_4 + 0{\cdot}2251B_2A_5], \tag{B 14}$$

where

$$A_1 = \frac{1}{(1+R'^2)^{\frac{1}{2}}}, \quad A_2 = \frac{-n_2R'}{(n_2^2+n_3^2)^{\frac{1}{2}}(1+R'^2)^{\frac{1}{2}}}, \quad A_3 = \frac{n_3}{(n_2^2+n_3^2)^{\frac{1}{2}}},$$

$$A_4 = \frac{-n_3R'}{(n_2^2+n_3^2)^{\frac{1}{2}}(1+R'^2)^{\frac{1}{2}}}, \quad A_5 = \frac{-n_2}{(n_2^2+n_3^2)^{\frac{1}{2}}},$$

$$A_6 = n_1A_1 + n_2A_2 + n_3A_4,$$

$$A_8 = A_1(C_{11}A_1 + C_{12}A_2 + C_{13}A_4 + C_{21}A_2 + C_{31}A_4) + A_2(C_{22}A_2 + C_{23}A_4 + C_{32}A_4) + C_{33}A_4^2,$$

$$A_9 = A_3(C_{22}A_3 + C_{23}A_5 + C_{32}A_5) + C_{33}A_5^2,$$

$$A_{10} = A_1(C_{12}A_3 + C_{13}A_5 + C_{21}A_3 + C_{31}A_5) + 2C_{33}A_4A_5 + A_2(2C_{22}A_3 + C_{23}A_5 + C_{32}A_5) + A_3(C_{23}A_4 + C_{32}A_4),$$

$$B_1 = A_6A_8, \quad B_2 = A_6A_{10}, \quad B_3 = A_6A_9,$$

with all quantities again evaluated at $\mathbf{x}^{(m)}$.

REFERENCES

Anczurowski, E. & Mason, S. G. 1968 Particle motions in sheared suspensions. IV. Rotation of rigid spheroids and cylinders. *Trans. Soc. Rheol.* **12**, 209.

Batchelor, G. K. 1970 Slender-body theory for particles of arbitrary cross-section in Stokes flow. *J. Fluid Mech.* **44**, 419.

Bowen, B. D. & Masliyah, J. H. 1973 Drag force on isolated axisymmetric particles in Stokes flow. *Can. J. Chem. Engng*, **51**, 8.

Brenner, H. 1964*a* The Stokes resistance of a slightly deformed sphere. *Chem. Engng Sci.* **19**, 519.

Brenner, H. 1964*b* The Stokes resistance of an arbitrary particle. III. Shear fields. *Chem. Engng Sci.* **19**, 631.

Brenner, H. 1966 Hydrodynamic resistance of particles. *Adv. in Chem. Eng.* **6**, 287.

Chang, Y. P., Kang, C. S. & Chen, D. J. 1973 The use of fundamental Green's functions for the solution of problems of heat conduction in anisotropic media. *Int. J. Heat Mass Transfer*, **16**, 1905.

Cox, R. G. 1970 The motion of long slender bodies in a viscous fluid. Part 1. General theory. *J. Fluid Mech.* **44**, 791.

Cox, R. G. 1971 The motion of long slender bodies in a viscous fluid. Part 2. Shear flow. *J. Fluid Mech.* **45**, 625.

Cruse, T. A. 1969 Numerical solutions in three-dimensional elastostatics. *Int. J. Solids Struct.* **5**, 1259.

Finlayson, B. A. 1972 *The Method of Weighted Residuals and Variational Principles.* Academic.

GLUCKMAN, M. J., WEINBAUM, S. & PFEFFER, R. 1972 Axisymmetric slow viscous flow past an arbitrary convex body of revolution. *J. Fluid Mech.* **55**, 677.

GOLDSMITH, H. L. & MASON, S. G. 1967 The microrheology of dispersions. In *Rheology* (ed. Eirich), pp. 85–250. Academic.

GÜNTER, N. M. 1967 *Potential Theory and Its Application to Basic Problems of Mathematical Physics.* Ungar.

HARRIS, J. B. & PITTMAN, J. F. T. 1975 Equivalent ellipsoidal axis ratios of slender rod-like particles. *J. Colloid Interface Sci.* **50**, 280.

HUNT, B. H. 1968 Numerical solution of an integral equation for flow from a circular orifice. *J. Fluid Mech.* **31**, 361.

JEFFERY, G. B. 1922 The motion of ellipsoidal particles immersed in a viscous fluid. *Proc. Roy. Soc.* A **102**, 161.

KANTOROVICH, L. V. & KRYLOV, V. I. 1958 *Approximate Methods of Higher Analysis.* Interscience.

LADYZHENSKAYA, O. A. 1963 *The Mathematical Theory of Viscous Incompressible Flow.* Gordon & Breach.

LAMB, H. 1932 *Hydrodynamics.* Cambridge University Press.

NIR, A. & ACRIVOS, A. 1973 On the creeping motion of two arbitrary-sized touching spheres in a linear shear field. *J. Fluid Mech.* **59**, 209.

OBERBECK, A. J. 1876 Über stationäre Flüssigkeitsbewgungen mit Berücksichtigung der inner Reibung. *J. reine angew. Math.* **81**, 62.

O'BRIEN, V. 1968 Form factors for deformed spheroids in Stokes flow. *A.I.Ch.E. J.* **14**, 870.

ODQVIST, F. K. G. 1930 Über die Randwertaufgaben der Hydrodynamik Zäher Flüssigkeiten. *Math. Z.* **32**, 329.

PAYNE, L. E. & PELL, W. H. 1960 The Stokes flow problem for a class of axially symmetric bodies. *J. Fluid Mech.* **7**, 529.

ROSEN, A. L. 1972 A computational algorithm for the Stokes problem. I. Methodology. *J. Inst. Math. Appl.* **9**, 265.

SAMPSON, R. A. 1891 On Stokes's current function. *Phil. Trans.* A **182**, 449.

SMITH, A. M. O. & HESS, J. L. 1966 Calculation of potential flow about arbitrary bodies. *Prog. Aero. Sci.* **8**, 1.

STOKES, G. G. 1851 On the effect of the internal friction of fluids on pendulums. *Trans. Camb. Phil. Soc.* **9**, 8.

TAYLOR, T. D. & ACRIVOS, A. 1964 The Stokes flow past an arbitrary particle – the slightly deformed sphere. *Chem. Engng Sci.* **19**, 445.